# Morphology controlled surface sulfurized $CoMn_2O_4$ microspikes electrocatalyst for water splitting with excellent OER rate for binder-free electrocatalytic oxygen evolution

Ali Bahadur[1,2†*], Waseem Hussain[3†], Shahid Iqbal[4†*], Farman Ullah[2], Muhammad Shoaib[5], Guocong Liu[4*], Kejun Feng[4]

[1]*Department of Transdisciplinary Studies, Graduate School of Convergence Science and Technology, Seoul National University, Seoul, 08826, South Korea*

[2]*Department of Chemistry, Quaid-i-Azam University, Islamabad, 45320, Pakistan.*

[3]*Department of Physics, Quaid-i-Azam University, Islamabad, 45320, Pakistan.*

[4]*School of Chemistry and Materials Engineering, Huizhou University, Huizhou 516007, Guangdong China.*

[5]*Department of Chemistry, Government Postgraduate College Samanabad Faisalabad 38000, Pakistan.*

***To whom correspondence should be addressed***

shahidiqbal@hzu.edu.cn (Shahid Iqbal) and gcl_109@163.com (Guocong Liu), alibahadur138@snu.ac.kr (Ali Bahadur)

† Authors have equal contribution

**Table S1** OER activity comparison with previously reported $CoMn_2O_4$ based electrocatalysts.

| Electrocatalyst | Synthesis route | Electrolyte concentration (KOH) | Catalyst Loading (mg cm$^{-2}$) | Potential mV @ 10 mA cm$^{-2}$ (vs. RHE) | Tafel slope (mV dec$^{-1}$) | Reference |
|---|---|---|---|---|---|---|
| **10S-$CoMn_2O_4$/FTO** | **Electrodeposition** | **0.1 M** | **0.3** | **300** | **26.28** | **This work** |
| **$CoMn_2O_4$/FTO** | **Electrodeposition** | **0.1 M** | **0.3** | **310** | **93.45** | **This work** |
| $CoMn_2O_4$ nanodots/rGO | Hot injection & Heating up method | 0.1 M | 0.319 | 310 | 56 | [1] |
| Mn3O4@$CoMn_2O_4$–$Co_xOy$ | One-pot two-step method | 0.1 M | 275 | 310 | 81 | [2] |
| $Mn_xCo_{3-x}O_4$ Spinel oxides | Sol-gel method | 1 M | 1.3 | 327 | 79 | [3] |
| $CoMn_2O_4$/N doped porous carbon | Solvothermal | 0.1 M | 0.33 | 570 | Not given | [4] |

**Table S2** OER activity comparison with recently reported (2020) oxides based electrocatalysts.

| Electrocatalyst | Electrolyte concentration (KOH) | Catalyst Loading (mg cm$^{-2}$) | Potential mV @ 10 mA cm$^{-2}$ (vs. RHE) | Tafel slope (mV dec$^{-1}$) | Reference |
|---|---|---|---|---|---|
| **10S-$CoMn_2O_4$/FTO** | **0.1 M** | **0.3** | **300** | **26.28** | **This work** |
| **$CoMn_2O_4$/FTO** | **0.1 M** | **0.3** | **310** | **93.45** | **This work** |
| $Ba_4Sr_4(Co_{0.8}Fe_{0.2})_4O_{15}$ | 0.1 M | 0.232 | 340 | 47 | [5] |
| Mixed Ni-Co-Mn oxides | 1 M | 0.12 | 400 | 74 | [6] |
| Defect-rich Cobalt oxide | 1 M | 0.12 | 369 | 46 | [7] |
| $Co_3O_4/MnCO_3$ | 1 M | Not given | 273 | 62.06 | [8] |
| $LiNi_{0.5}Co_{0.2}Mn_{0.3}O_2$ | 0.1 M | 0.26 | ~480 | 51.9 | [9] |
| Mn–CoO@$Fe(OH)_3$/NF | 1 M | Not given | 195 | 49 | [10] |
| $Co_aFe_bV_cO_x$ | 1 M | 0.2 | 249 | 41 | [11] |
| Co-Fe oxides/carbon paper | 1 M | Not given | 460 | 105 | [12] |
| Cobalt Iron oxide nanowires | 1 M | 0.12 | 378 | 54 | [13] |
| $Fe_{0.5}Co_{0.5}MoO_{4-x}S_x$ nanoflowers | 1 M | Not given | 263 | 87 | [14] |
| La-doped $CoO_x$ NSs | 0.1 M | Not given | 353 | 78.2 | [15] |

**Supplementary Note: 1**

Electrocatalytic activity surface area (ECSA) estimation:

ECSA was estimated by equation: ECSA = $C_{dl}/C_s$, where $C_s$ denotes specific capacitance of 1 $cm^2$ of real surface (assumed to be 0.4 $mF/cm^2$ in this study) while $C_{dl}$ denotes double-layer capacitance. Cyclic voltammetry was performed at different scan rates (1, 2, 3, 4, 5, 6, 7, 8, 9, and 10 mV/s) in the non-Faradaic region (1.015 -1.065 vs. RHE). ECSA was estimated directly from $C_{dl}$ by plotting $\Delta j$ ($\Delta j$ = ja-jc) as a function of scan rate.

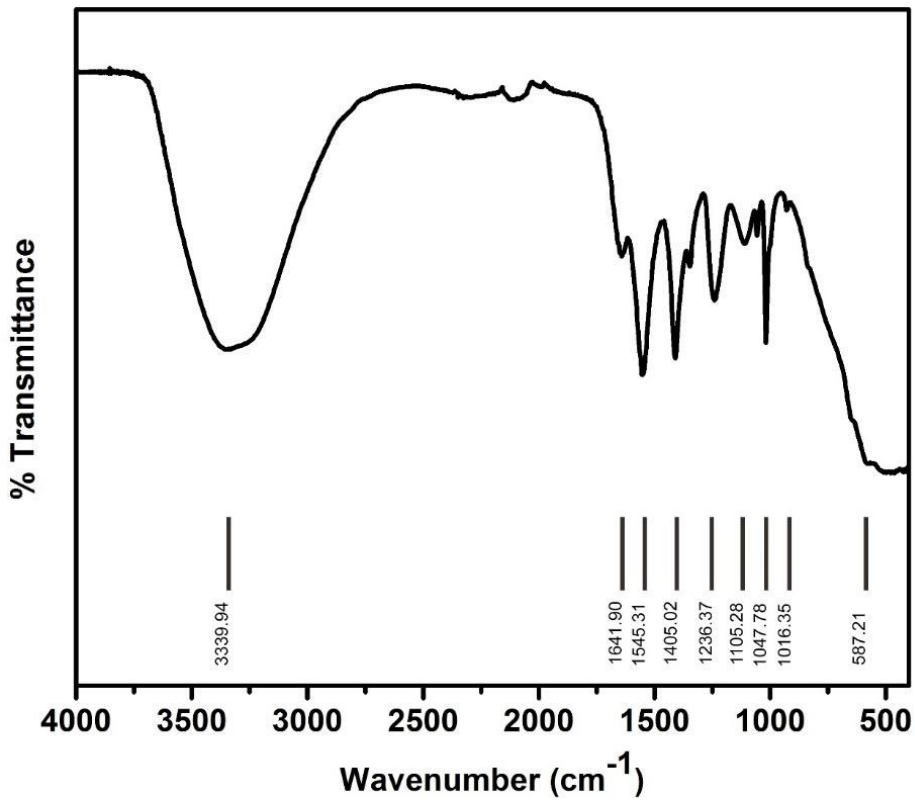


**Figure S1** FTIR spectra of synthesized $CoMn_2O_4$@FTO substrate.

FTIR spectra displayed absorption bands around 3700 -2690 and 1641 $cm^{-1}$, attributed to the stretching vibrations of OH and the bending vibrations of H-O-H from water molecules on the surface and this is consistent with the published data.[16] Importantly, the characteristic peak above 500 $cm^{-1}$ and at 1105.28 $cm^{-1}$ confirm the spinel structure of the product. Moreover, the absorption band appearing at 401 $cm^{-1}$ can be ascribed to the vibration of Co-O-Mn.[17]

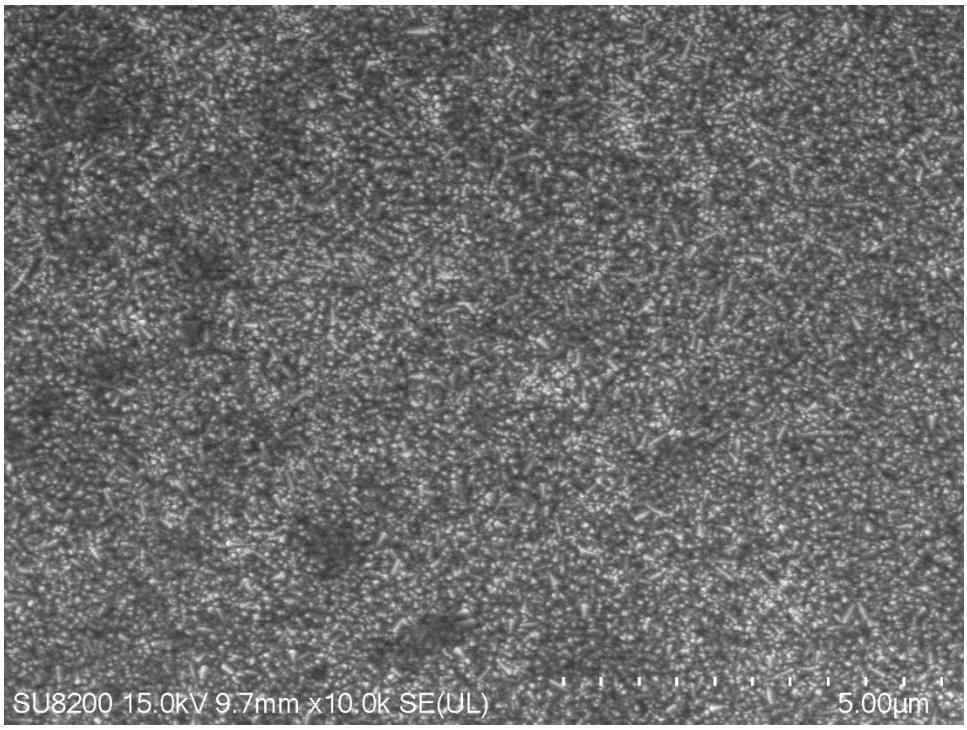


**Figure S2** SEM micrographs of Bare FTO.

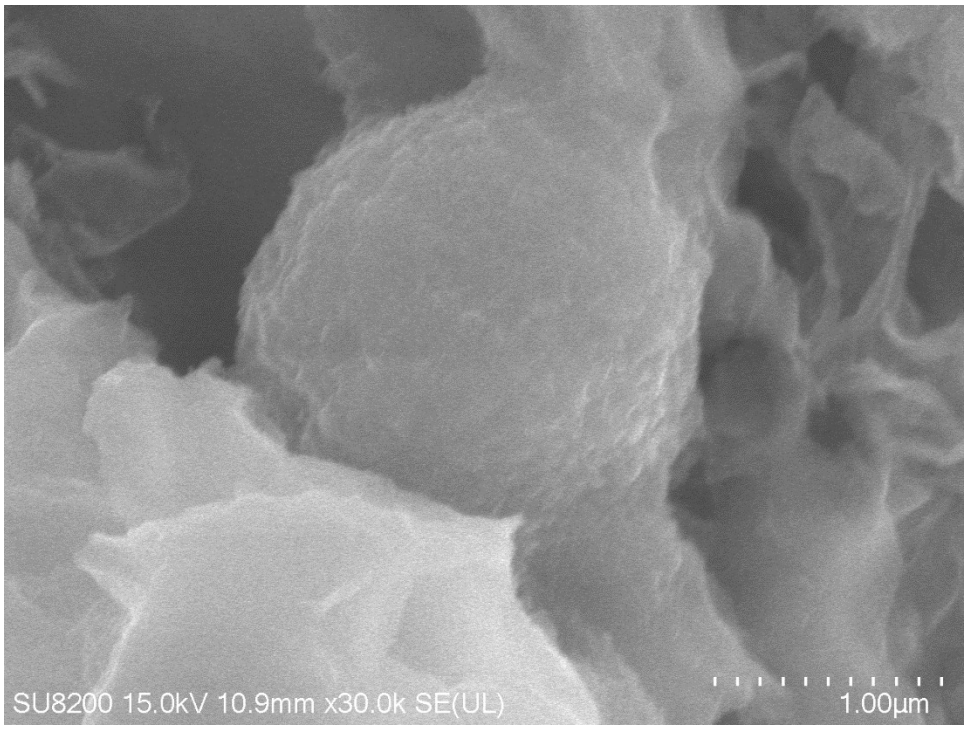


**Figure S3** High magnification SEM image of $Co_3O_4$@FTO.

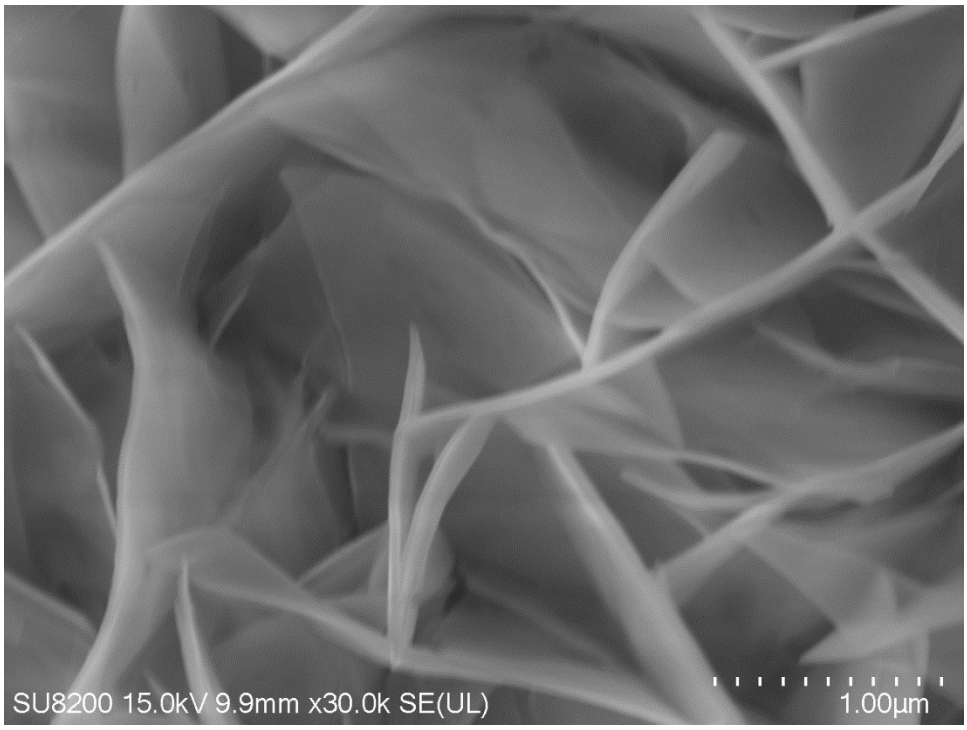


**Figure S4** High magnification SEM image of $Mn_3O_4$@FTO.

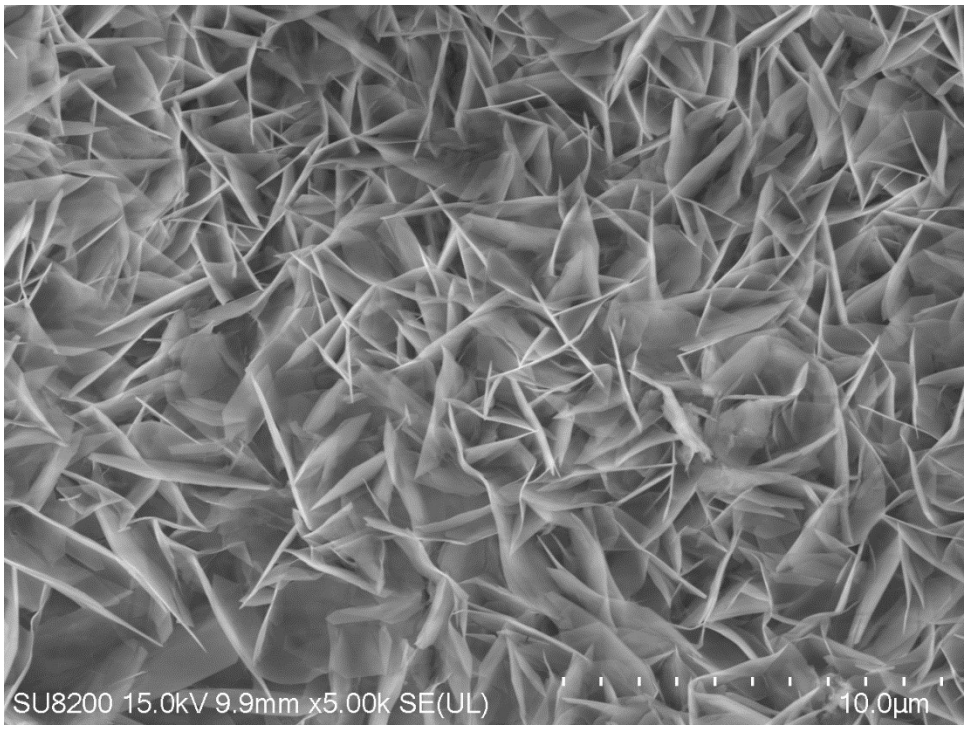


**Figure S5** High magnification SEM image of $Mn_3O_4$@FTO.

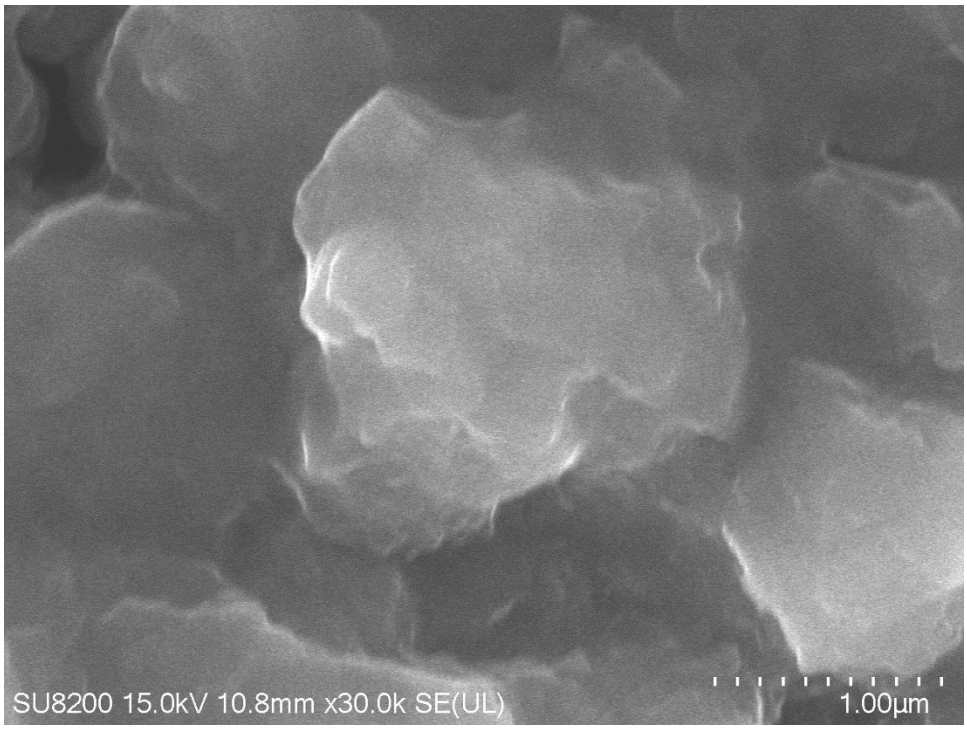


**Figure S6** High magnification SEM image of $CoMn_2O_4$@FTO.

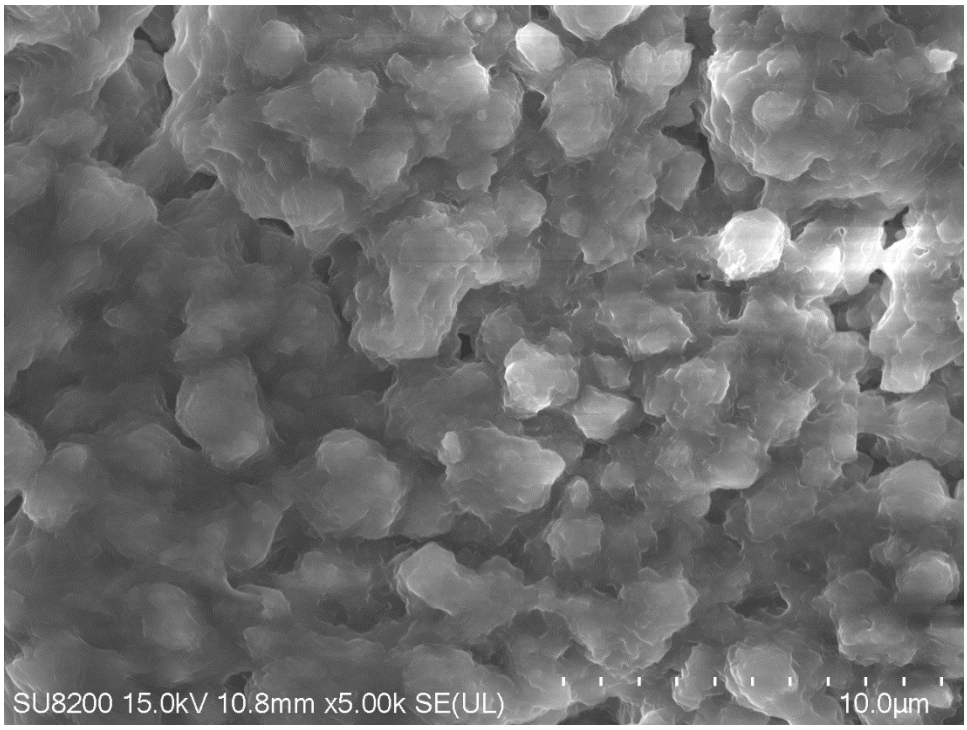


**Figure S7** Low magnification SEM image of $CoMn_2O_4$@FTO.

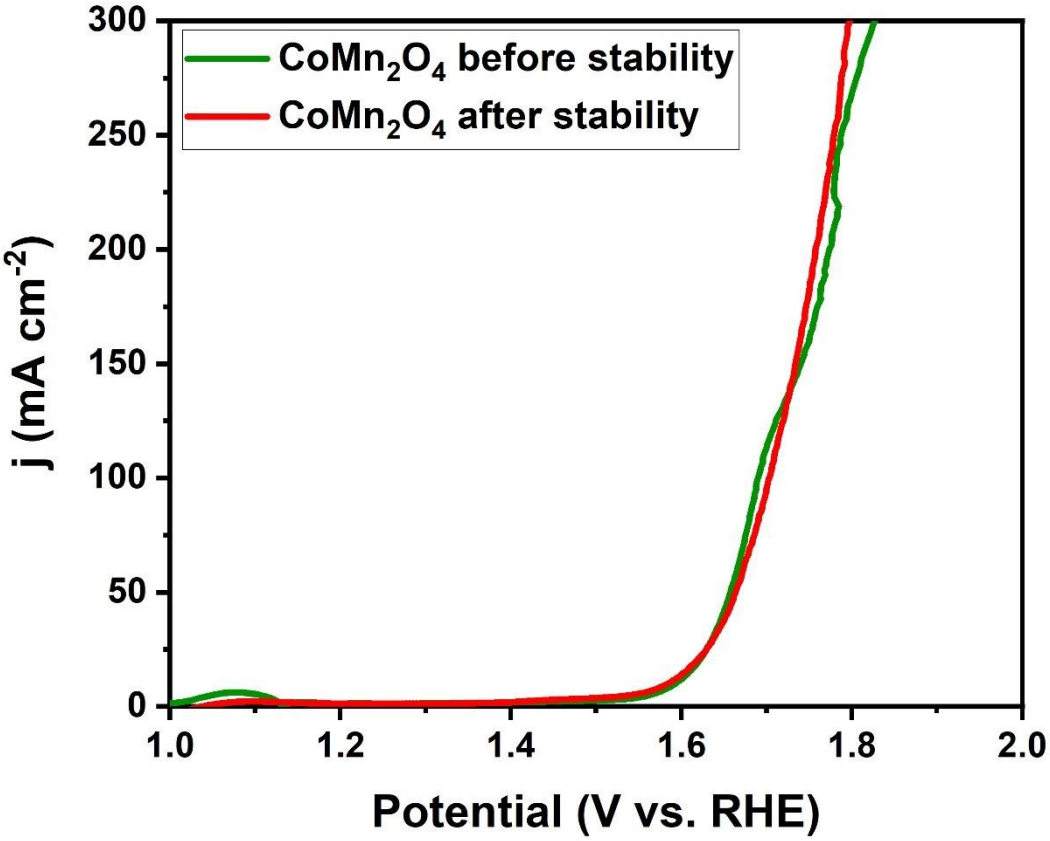


**Figure S8** OER activity comparison of $CoMn_2O_4$@FTO before and after stability (24 h at 20 mA $cm^{-2}$) in 0.1 M KOH solution.

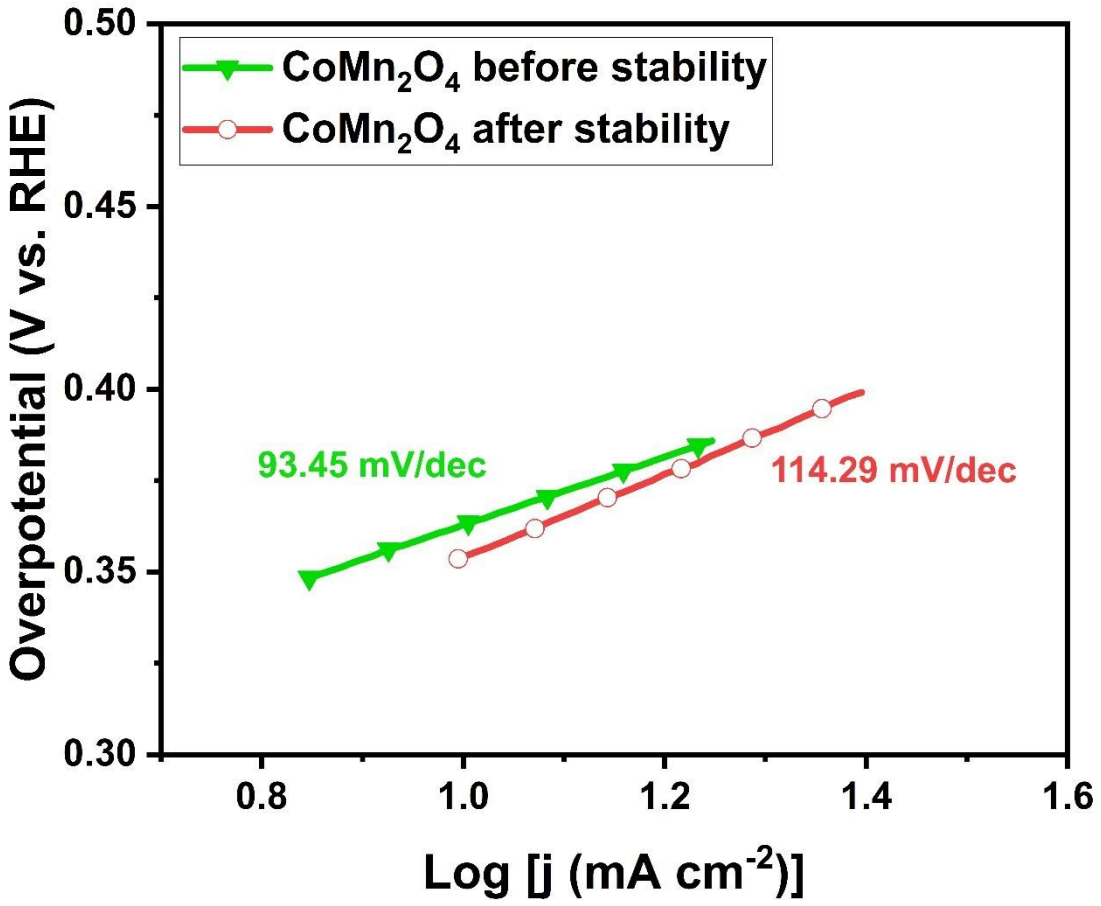


**Figure S9** Tafel slopes for $CoMn_2O4$@FTO before and after 24 h stability test in 0.1 M KOH solution.

**Table S3** Electrocatalytic OER performance for electrodeposited material at FTO substrate at higher current density values.

| Sample | E(mV) vs. RHE at 20 mA $cm^{-2}$ | E(mV) vs. RHE at 50 mA $cm^{-2}$ | E(mV) vs. RHE at 100 mA $cm^{-2}$ |
|---|---|---|---|
| $CoMn_2O_4$ | 380 | 420 | 450 |
| $Co_2MnO_4$ | 370 | 480 | 620 |
| $Co_3O_4$ | 530 | 880 | 1200 |
| $Mn_3O_4$ | 650 | 760 | 880 |

**Table S4** Electrochemical impedance spectroscopy (EIS) parameters.

| Sample | Solution resistance (Rs) / Ω | Charge transfer resistance (Rct) / Ω |
|---|---|---|
| $Co_3O_4$ | 18.88 | 15.43 |
| $Mn_3O_4$ | 15.63 | 14.29 |
| $Co_2MnO_4$ | 14.22 | 9.84 |
| $CoMn_2O_4$ | 12.12 | 5.51 |

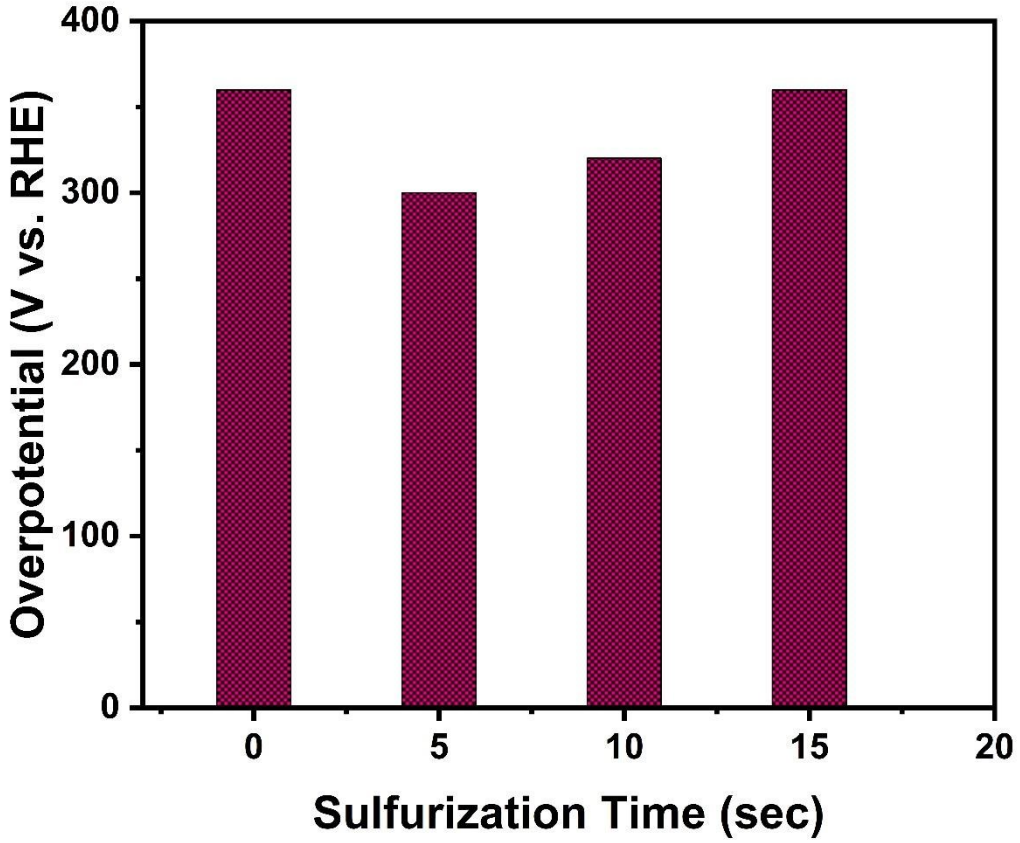


**Figure S10** Comparison of overpotential (at 10 mA $cm^{-2}$) with varying sulfurization time.

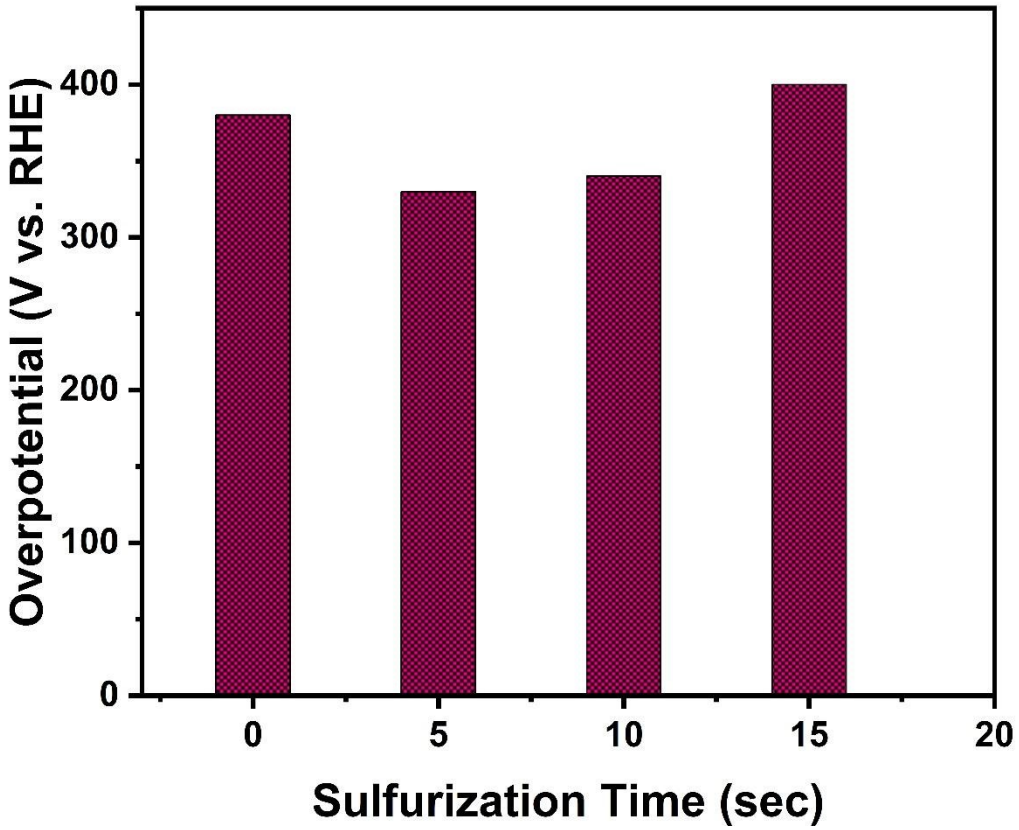


**Figure S11** Comparison of overpotential (at 20 mA $cm^{-2}$) with varying sulfurization time.

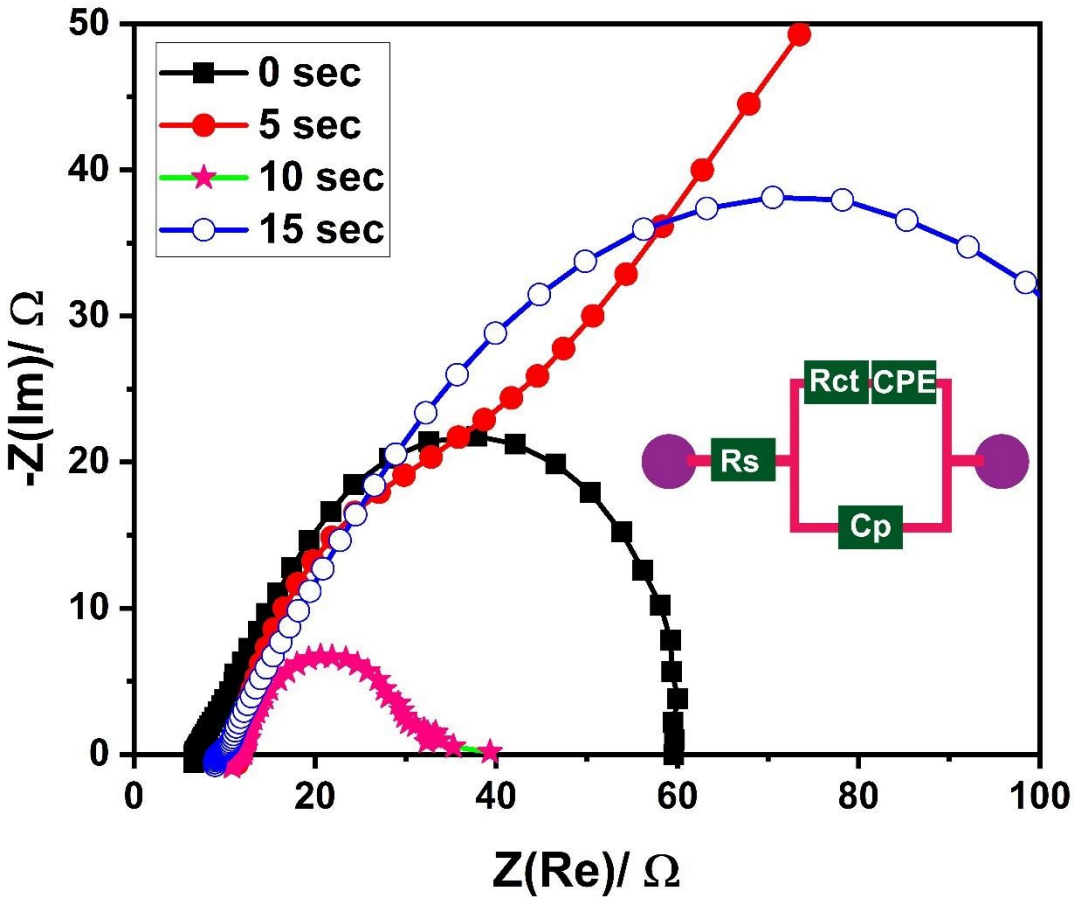


**Figure S12** Nyquist plot of S-$CoMn_2O_4$@FTO with different sulfurization times (inset shows the circuit diagram).

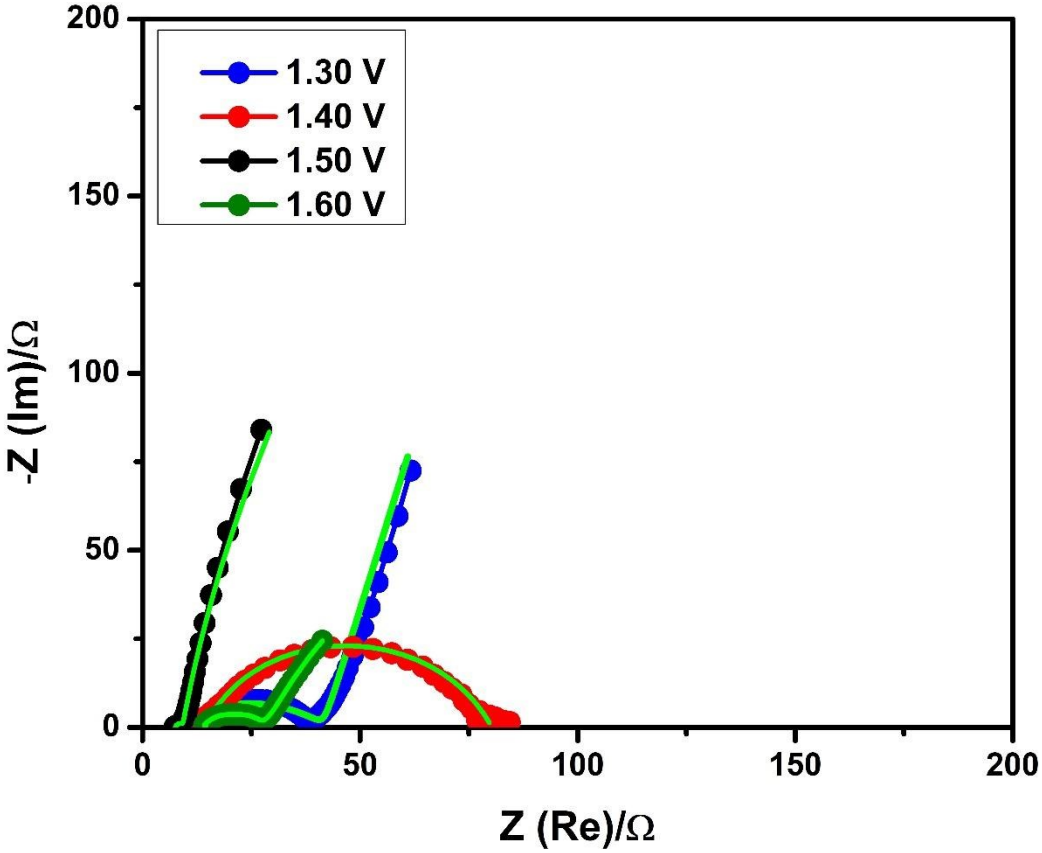


**Figure S13** Nyquist plot of S-$CoMn_2O_4$@FTOat different biases (inset shows the circuit diagram).

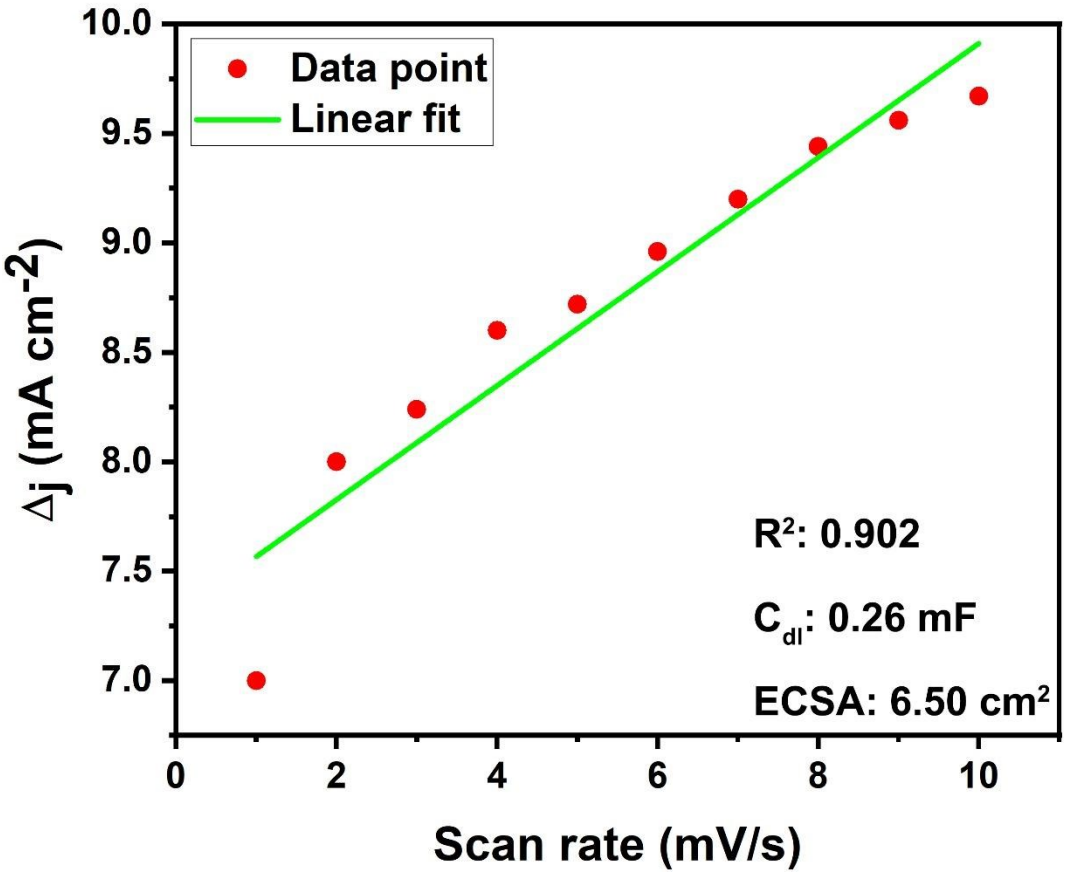


**Figure S14** Double-layer capacitance ($C_{dl}$) and electrochemical surface area calculation by plotting Δj (ja-jc) as a function of scan rate.

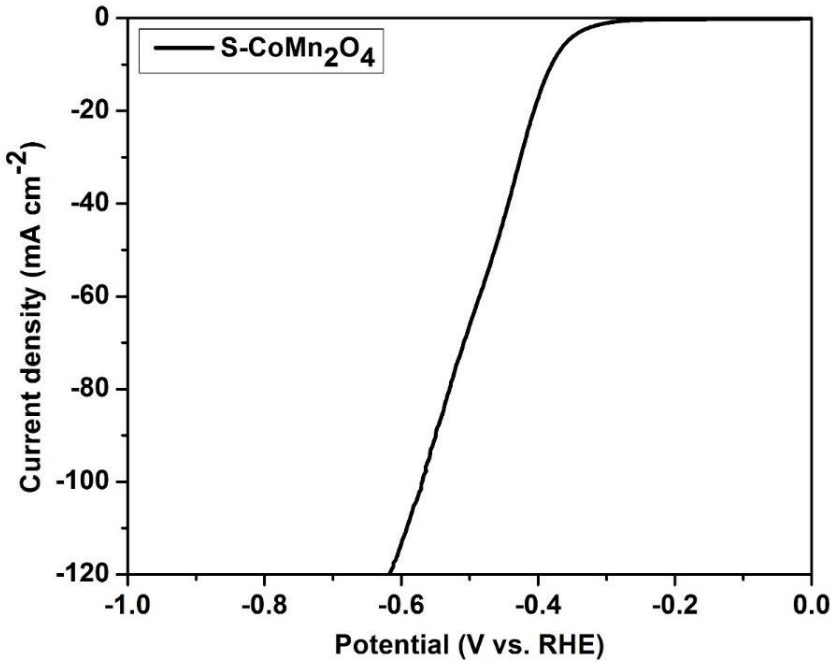


**Figure S15** HER activity of S-$CoMn_2O_4$-MFs@FTO in 0.5 M $H_2SO_4$ solution.

Electrodeposited material (S-$CoMn_2O_4$-MFs@FTO) was also tested for hydrogen evolution reaction (HER) and the synthesized material showed no or very little HER activity with an overpotential of 380 and 403 mV at 10 mA $cm^{-2}$, respectively.

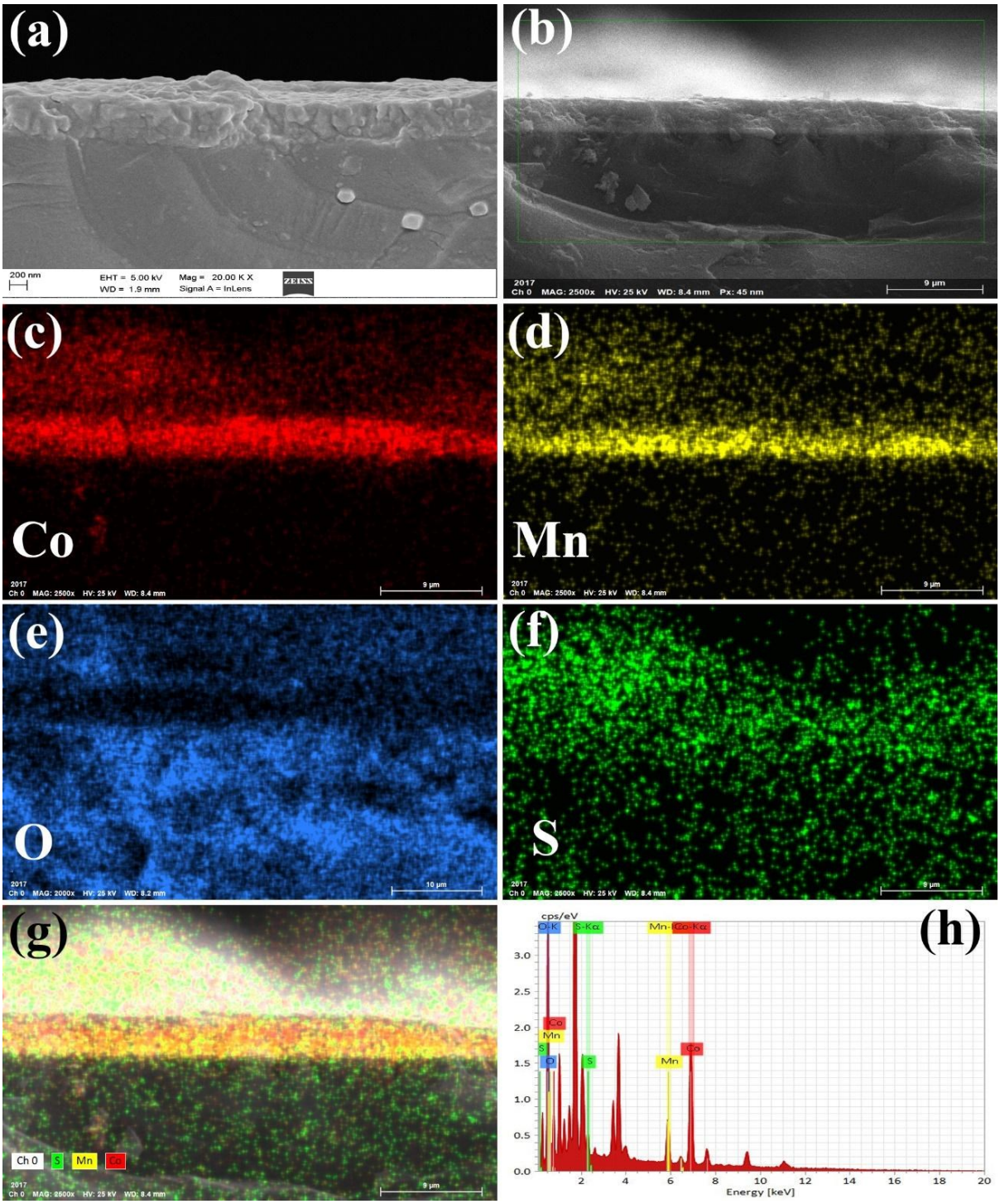


**Figure S16** Cross-sectional SEM images of surface sulfurized $CoMn_2O_4$ microspikes (a). STEM image (b) of surface sulfurized $CoMn_2O_4$ microspikes and elemental mapping of (c) Co; (d) Mn; (e) O; (f) S and (g) combine mapping. (h) EDX of surface sulfurized $CoMn_2O_4$ microspikes.

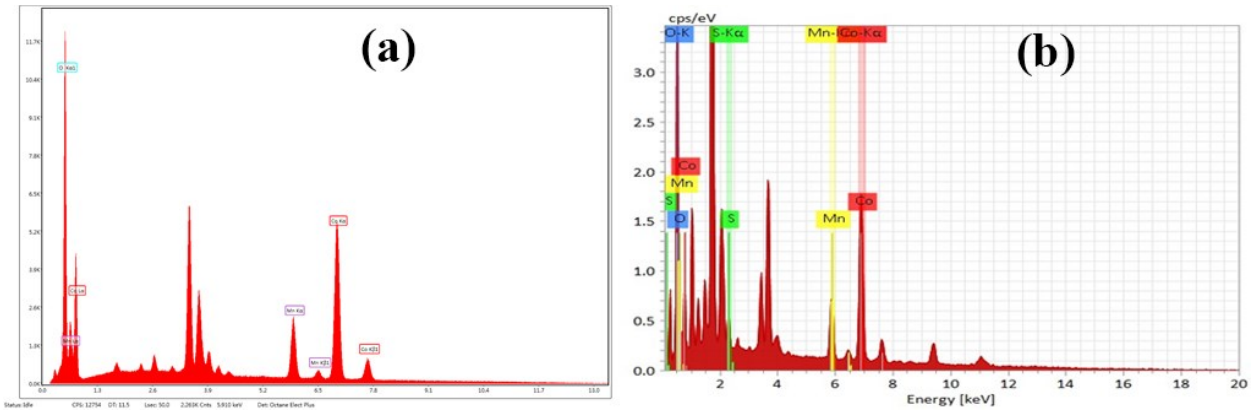


**Figure S17** EDX data of $CoMn_2O_4$ microspikes before (a) and after sulfurization (b).

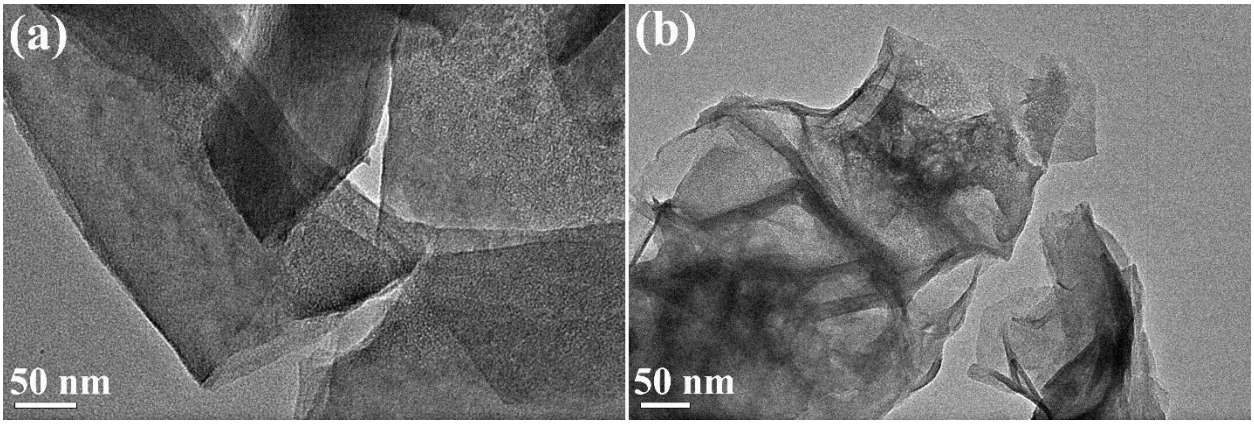


**Figure S18** HRTEM images of surface sulfurized $CoMn_2O_4$ microspikes (a) before (b) and after electrocatalysis reaction .

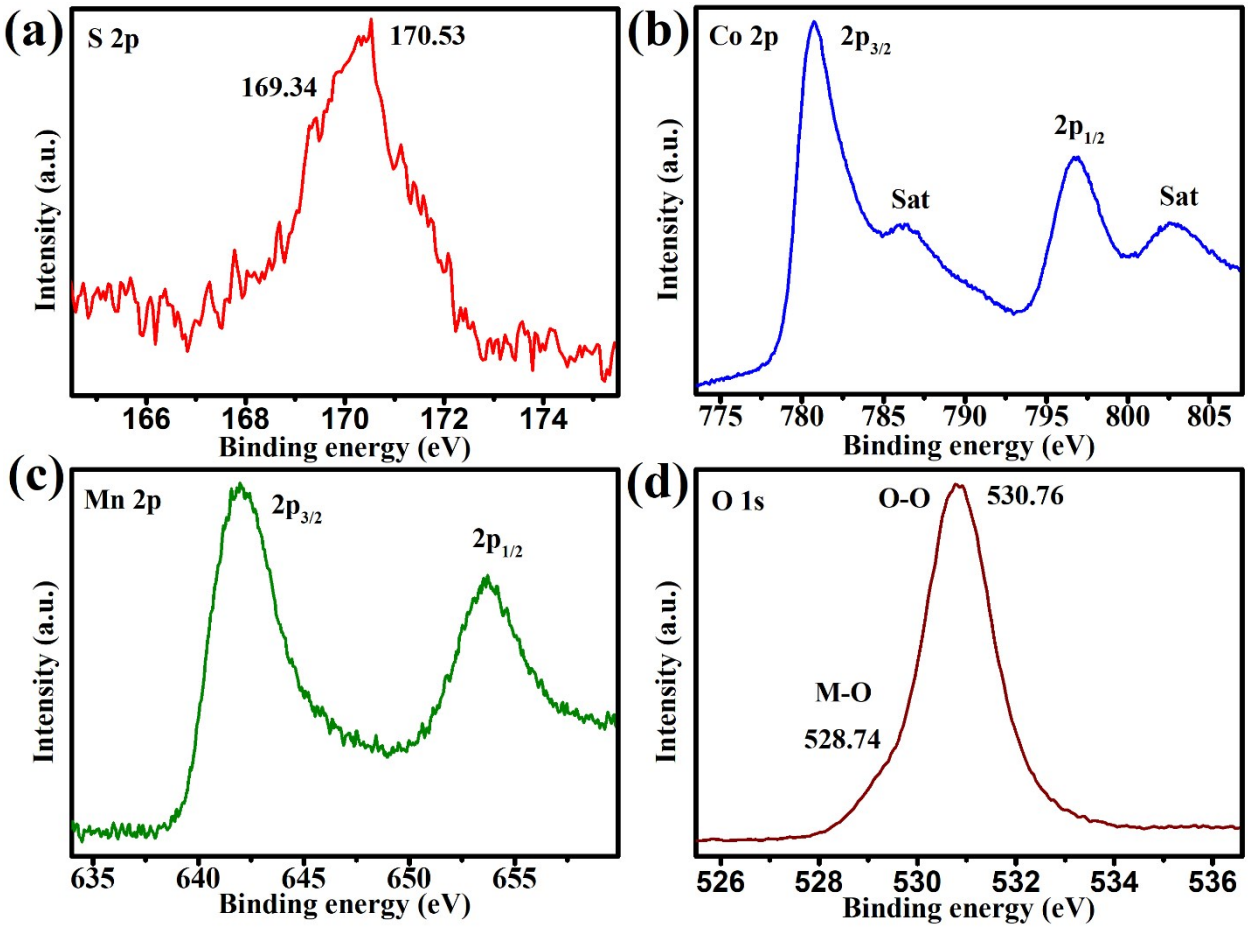


**Figure S19** High-resolution XPS spectra of surface sulfurized $CoMn_2O_4$ microspikes after electrocatalysis reaction. (a) S 2p; (b) Co 2p; (c) Mn 2p; (d) O 1s.

**Table S5** XPS data of surface sulfurized $CoMn_2O_4$ microspikes and actual values of peak area of XPS fitting results.

| Sr. No. | Name | Start BE | Peak BE | End BE | Height CPS | FWHM eV | Area (P) CPS. eV | Area (N) TPP-2M | Atomic % |
|---|---|---|---|---|---|---|---|---|---|
| 1 | C 1s | 297.96 | 284.8 | 279.06 | 22467.07 | 1.39 | 36508.33 | 511.93 | 24.24 |
| 2 | C 1s Scan A | 297.96 | 288.58 | 279.06 | 4150.89 | 1.39 | 6745.07 | 94.81 | 4.49 |
| 3 | C 1s Scan B | 297.96 | 286.38 | 279.06 | 3113.88 | 1.39 | 5059.97 | 71.02 | 3.36 |
| 4 | O 1s | 544.86 | 531.2 | 525.93 | 81060.53 | 1.73 | 170677.21 | 989.59 | 46.85 |
| 5 | Co 2p | 811.96 | 780.84 | 771.06 | 26578.41 | 3.49 | 211591.87 | 242.77 | 11.49 |
| 6 | Mn 2p | 659.96 | 641.52 | 632.06 | 18688.56 | 3.47 | 106919.91 | 158.51 | 7.5 |
| 7 | S 2p | 174.96 | 168.16 | 157.06 | 1478.75 | 2.09 | 6293.72 | 43.68 | 2.07 |

## REFERENCES


[1] J. Du, C. Chen, F. Cheng, J. Chen, Rapid synthesis and efficient electrocatalytic oxygen reduction/evolution reaction of $CoMn_2O_4$ nanodots supported on graphene, Inorg. Chem. (2015). https://doi.org/10.1021/acs.inorgchem.5b00518.

[2] Z. Luo, E. Irtem, M. Ibánez, R. Nafria, S. MartÍ-Sánchez, A. Genç, M. De La Mata, Y. Liu, D. Cadavid, J. Llorca, J. Arbiol, T. Andreu, J.R. Morante, A. Cabot, $Mn_3O_4$@$CoMn_2O_4$-$Co_xO_y$ nanoparticles: Partial cation exchange synthesis and electrocatalytic properties toward the oxygen reduction and evolution reactions, ACS Appl. Mater. Interfaces. (2016). https://doi.org/10.1021/acsami.6b02786.

[3] K. Lankauf, K. Cysewska, J. Karczewski, A. Mielewczyk-Gryń, K. Górnicka, G. Cempura, M. Chen, P. Jasiński, S. Molin, $Mn_xCo_{3-x}O_4$ spinel oxides as efficient oxygen evolution reaction catalysts in alkaline media, Int. J. Hydrogen Energy. (2020). https://doi.org/10.1016/j.ijhydene.2020.03.188.

[4] J.L. Digol, M.F.M. Labata, M.F. Divinagracia, J.D. Ocon, $CoMn_2O_4$ anchored on N-doped high-dimensional hierarchical porous carbon derived from biomass for bifunctional oxygen electrocatalysis , ECS Trans. (2017). https://doi.org/10.1149/07711.0525ecst.

[5] Y. Zhu, H.A. Tahini, Z. Hu, Z.G. Chen, W. Zhou, A.C. Komarek, Q. Lin, H.J. Lin, C. Te Chen, Y. Zhong, M.T. Fernández-Díaz, S.C. Smith, H. Wang, M. Liu, Z. Shao, Boosting oxygen evolution reaction by creating both metal ion and lattice-oxygen active sites in a complex oxide, Adv. Mater. (2020). https://doi.org/10.1002/adma.201905025.

[6] T. Priamushko, R. Guillet-Nicolas, M. Yu, M. Doyle, C. Weidenthaler, H. Tuÿsüz, F. Kleitz, Nanocast Mixed Ni-Co-Mn oxides with controlled surface and pore structure for electrochemical oxygen evolution reaction, ACS Appl. Energy Mater. (2020). https://doi.org/10.1021/acsaem.0c00544.

[7] M. Yu, F. Waag, C.K. Chan, C. Weidenthaler, S. Barcikowski, H. Tüysüz, Laser Fragmentation-induced defect-rich cobalt oxide nanoparticles for electrochemical oxygen evolution reaction, ChemSusChem. (2020). https://doi.org/10.1002/cssc.201903186.

[8] G. Yang, B. Zhu, D. Gao, Y. Fu, J. Zhao, J. Li, A $Co_3O4/MnCO_3$ heterojunction on three-dimensional nickel foam for an enhanced oxygen evolution reaction, CrystEngComm. (2020). https://doi.org/10.1039/d0ce00325e.

[9] D. Huang, J. Yu, Z. Zhang, C. Engtrakul, A. Burrell, M. Zhou, H. Luo, R.C. Tenent,

Enhancing the Electrocatalysis of $LiNi_{0.5}Co_{0.2}Mn_{0.3}O_2$ by introducing lithium deficiency for oxygen evolution reaction, ACS Appl. Mater. Interfaces. (2020). https://doi.org/10.1021/acsami.9b22438.

[10] Z. Chen, Z. Hu, D. Zhu, Z. Feng, X. Li, J. Huang, X. Shen, Construction of hierarchical Mn–CoO@$Fe(OH)_3$ nanofiber array for oxygen evolution reaction, J. Alloys Compd. (2020). https://doi.org/10.1016/j.jallcom.2020.155560.

[11] J. Chen, H. Li, Z. Pei, Q. Huang, Z. Yuan, C. Wang, X. Liao, G. Henkelman, Y. Chen, L. Wei, Catalytic activity atlas of ternary Co–Fe–V metal oxides for the oxygen evolution reaction, J. Mater. Chem. A. (2020). https://doi.org/10.1039/d0ta04088f.

[12] M. Ishizaki, H. Fujii, K. Toshima, H. Tanno, H. Sutoh, M. Kurihara, Preparation of Co-Fe oxides immobilized on carbon paper using water-dispersible Prussian-blue analog nanoparticles and their oxygen evolution reaction (OER) catalytic activities, Inorganica Chim. Acta. (2020). https://doi.org/10.1016/j.ica.2019.119345.

[13] E. Budiyanto, M. Yu, M. Chen, S. DeBeer, O. Rüdiger, H. Tüysüz, Tailoring morphology and electronic structure of cobalt iron oxide nanowires for electrochemical oxygen evolution reaction, ACS Appl. Energy Mater. (2020). https://doi.org/10.1021/acsaem.0c01201.

[14] B. Fei, Z. Chen, Y. Ha, R. Wang, H. Yang, H. Xu, R. Wu, Anion-cation co-substitution activation of spinel $CoMoO_4$ for efficient oxygen evolution reaction, Chem. Eng. J. (2020). https://doi.org/10.1016/j.cej.2020.124926.

[15] X. Gu, H. Jing, X. Mu, H. Yang, Q. Zhou, S. Yan, S. Liu, C. Chen, La-triggered synthesis of oxygen vacancy-modified cobalt oxide nanosheets for highly efficient oxygen evolution

in alkaline media, J. Alloys Compd. (2020). https://doi.org/10.1016/j.jallcom.2019.152274.

[16] F. Chen, Y. Cao, D. Jia, A facile route for the synthesis of ZnS rods with excellent photocatalytic activity, Chem. Eng. J. 234 (2013) 223–231. https://doi.org/10.1016/j.cej.2013.08.075.

[17] S.A. Hosseini, A. Niaei, D. Salari, S.R. Nabavi, Nanocrystalline $AMn_2O_4$ ( A = Co , Ni , Cu ) spinels for remediation of volatile organic compounds — synthesis , characterization and catalytic performance, Ceram. Int. 38 (2012) 1655–1661. https://doi.org/10.1016/j.ceramint.2011.09.057.